

Electronic supplementary information:

Bright white light emitting Eu and Tb co-doped monodisperse In_2O_3 Nanocrystals

Sirshendu Ghosh, Kajari Das, Godhuli Sinha, J. Lahtinen and S. K. De

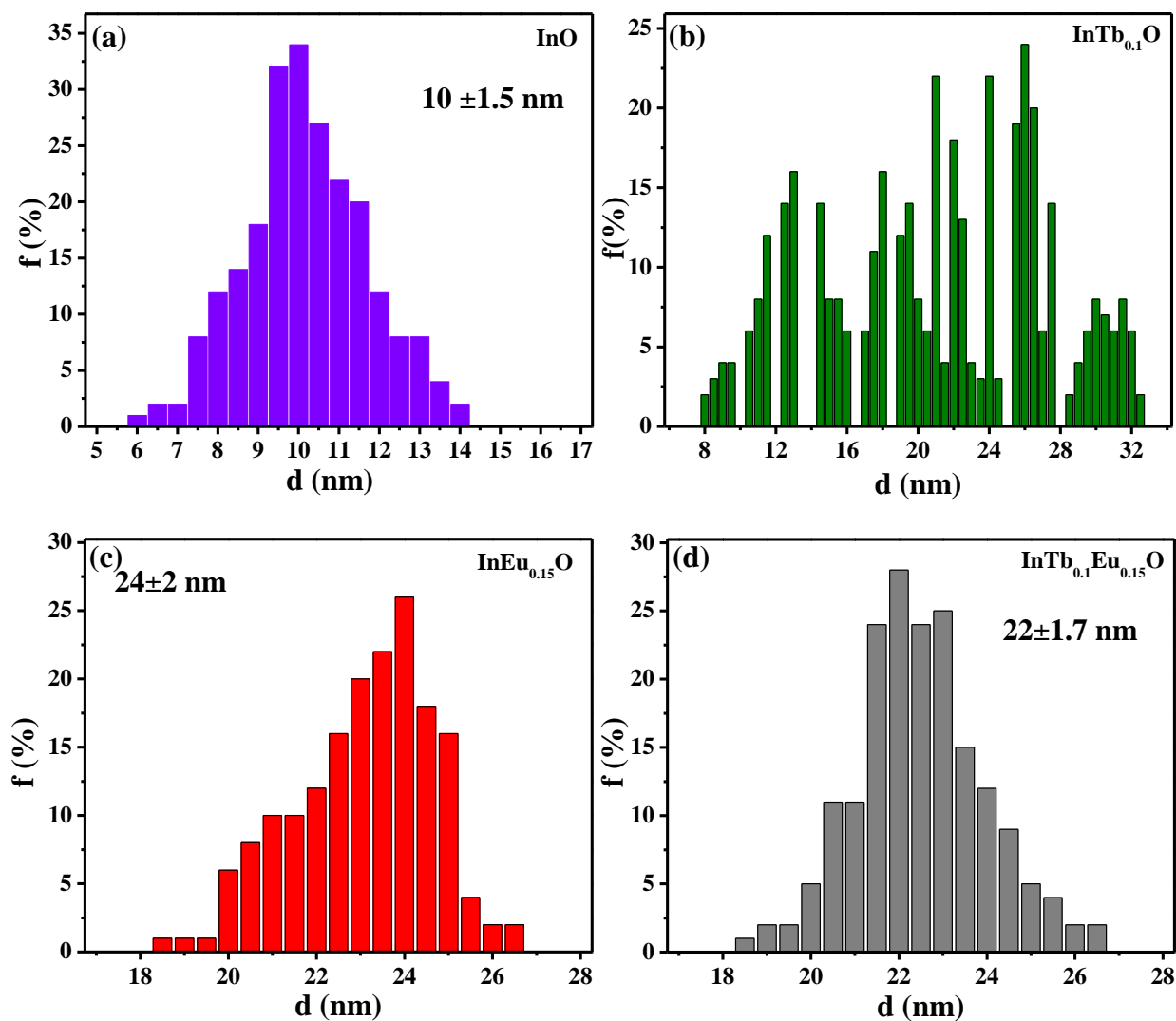


Fig. S1: Size distribution histograms for (a) InO , (b) $\text{InTb}_{0.1}\text{O}$, (c) $\text{InEu}_{0.15}\text{O}$ and (d) $\text{InTb}_{0.1}\text{Eu}_{0.15}\text{O}$ NCs. The histograms clearly show monodispersity of pure, Eu^{3+} and co-doped NCs and heterodispersity of Tb doped NCs. TEM images are reported in Fig. 2 of main article.

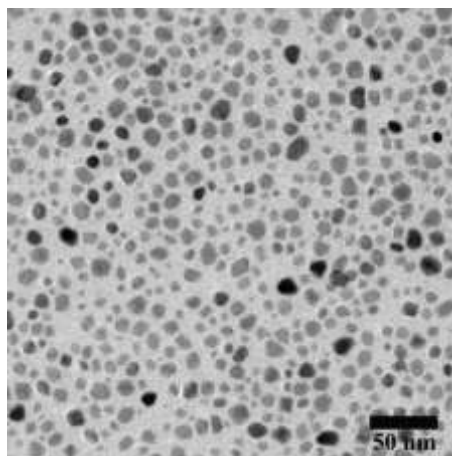
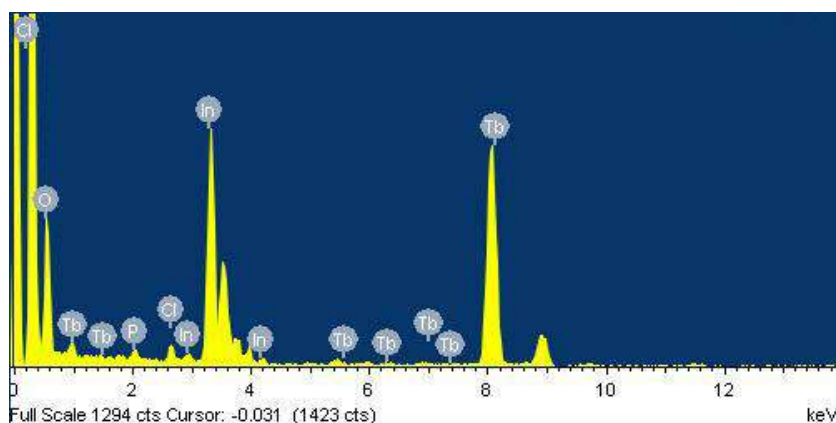


Fig. S2: TEM image of In_2O_3 NCs formed after 12 hr of reaction represents the colloidal stability and monodispersity for long time reaction.



Element	Peak Area	Area Sigma	k factor	Abs Corr.	Weight%	Weight% Sigma	Atomic%
O K	2528	95	1.810	1.000	20.64	0.73	63.33
P K	237	53	0.992	1.000	1.06	0.23	1.68
Cl K	382	53	0.964	1.000	1.66	0.23	2.30
In L	9445	224	1.782	1.000	75.90	0.86	32.46
Tb L	77	50	2.142	1.000	0.74	0.48	0.23
Totals					100.00		

Fig. S3: EDAX analysis shows the presence of chloride anion in $\text{InTb}_{0.05}\text{O}$ sample in a considerable amount.

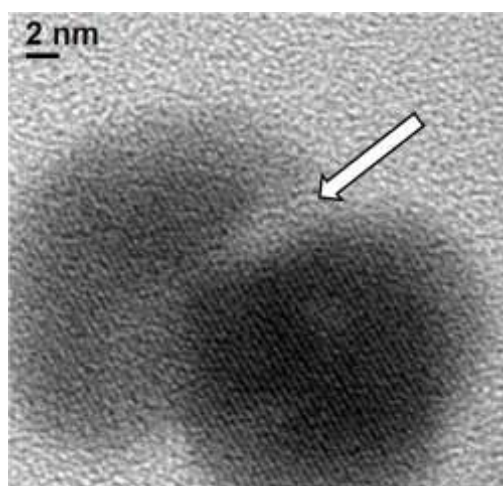


Fig. S4: HRTEM image of a NC of sample $\text{InEu}_{0.5}\text{O}$ shows the oriented attachment of two nanocrystals following the similar crystallographic orientation.

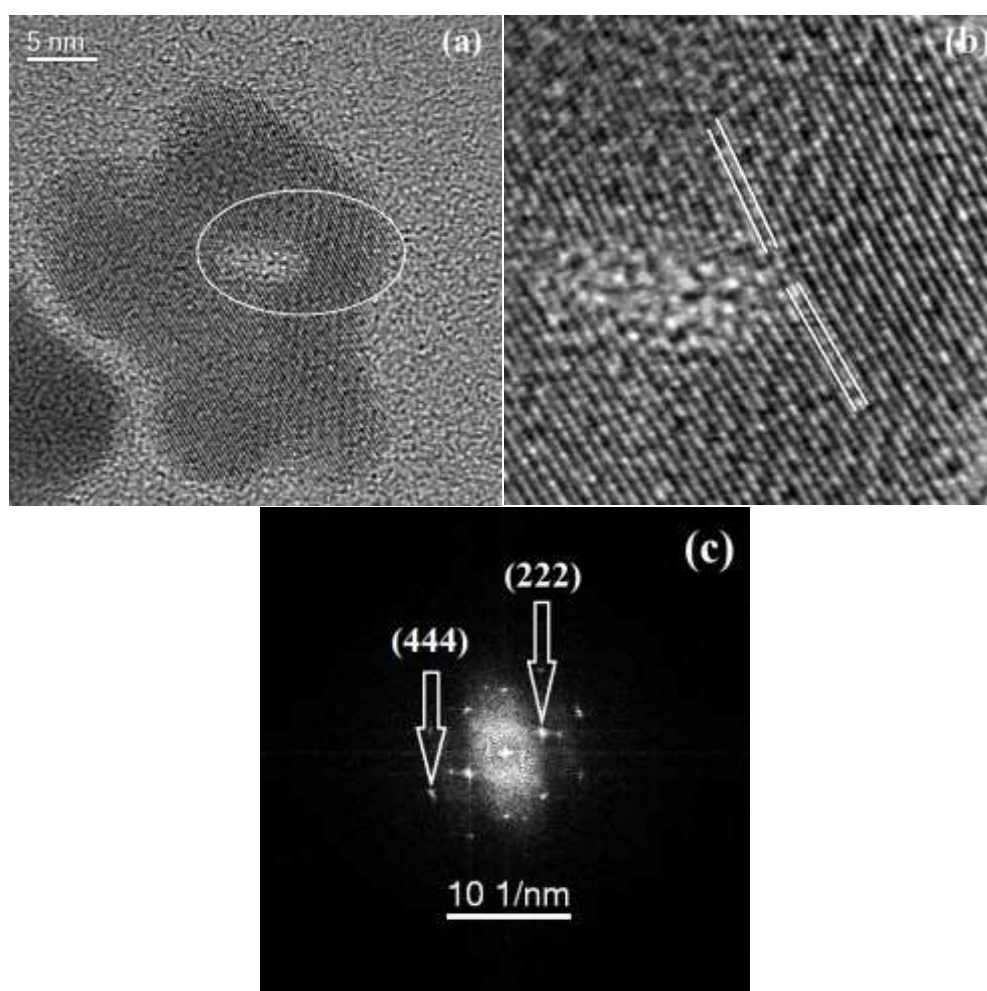


Fig. S5: (a) HRTEM image of $\text{InTb}_{0.1}\text{Eu}_{0.15}\text{O}$ sample clearly indicates the attachment of four NCs by oriented attachment. (b) The enlarged view of circular area shows the attachment of (222) planes of two NCs in a little twisted pattern for minimizing the surface energy. (c) FFT pattern of that area shown in the figure b indicates the presence of twin planes (222) and (444).

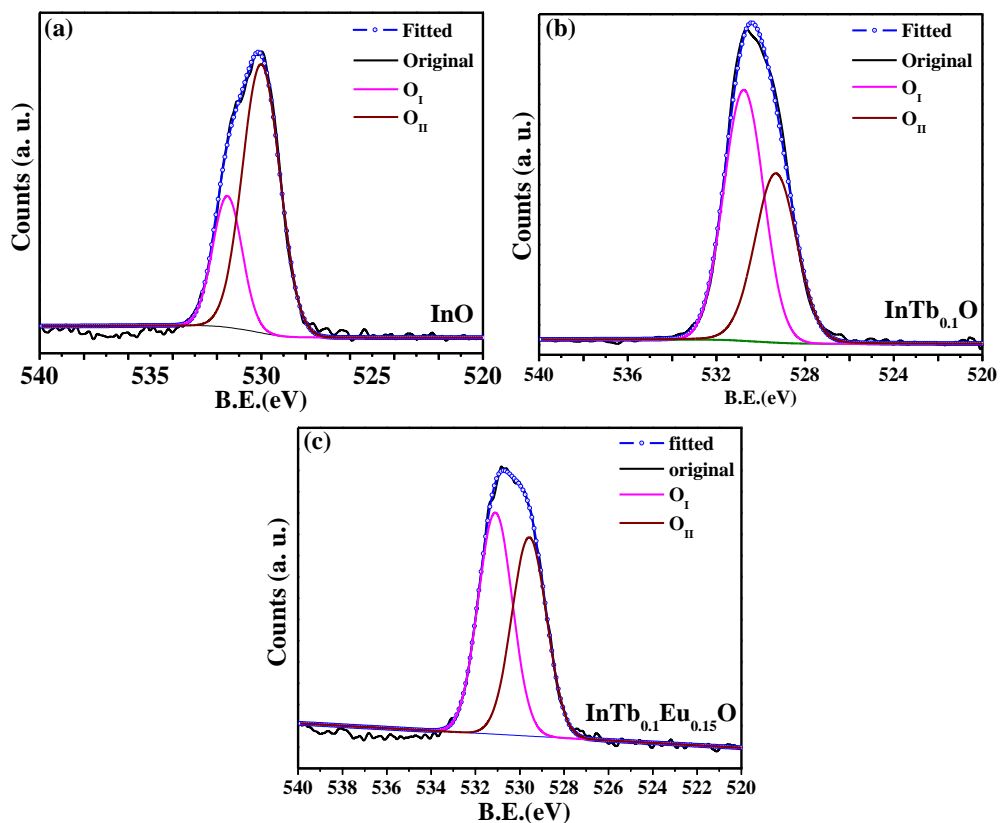


Fig. S6: XPS spectra for O 1S peak of (a) InO, (b) InTb_{0.1}O and (c) InTb_{0.1}Eu_{0.15}O nanocrystals. De-convolution of the peak results two peaks namely O_I and O_{II} for all samples. O_{II} peak is for O²⁻ situated with In³⁺ in crystal structure of In₂O₃. Whereas higher binding energy peak O_I is related to oxygen vacancy which is present in all the samples.¹

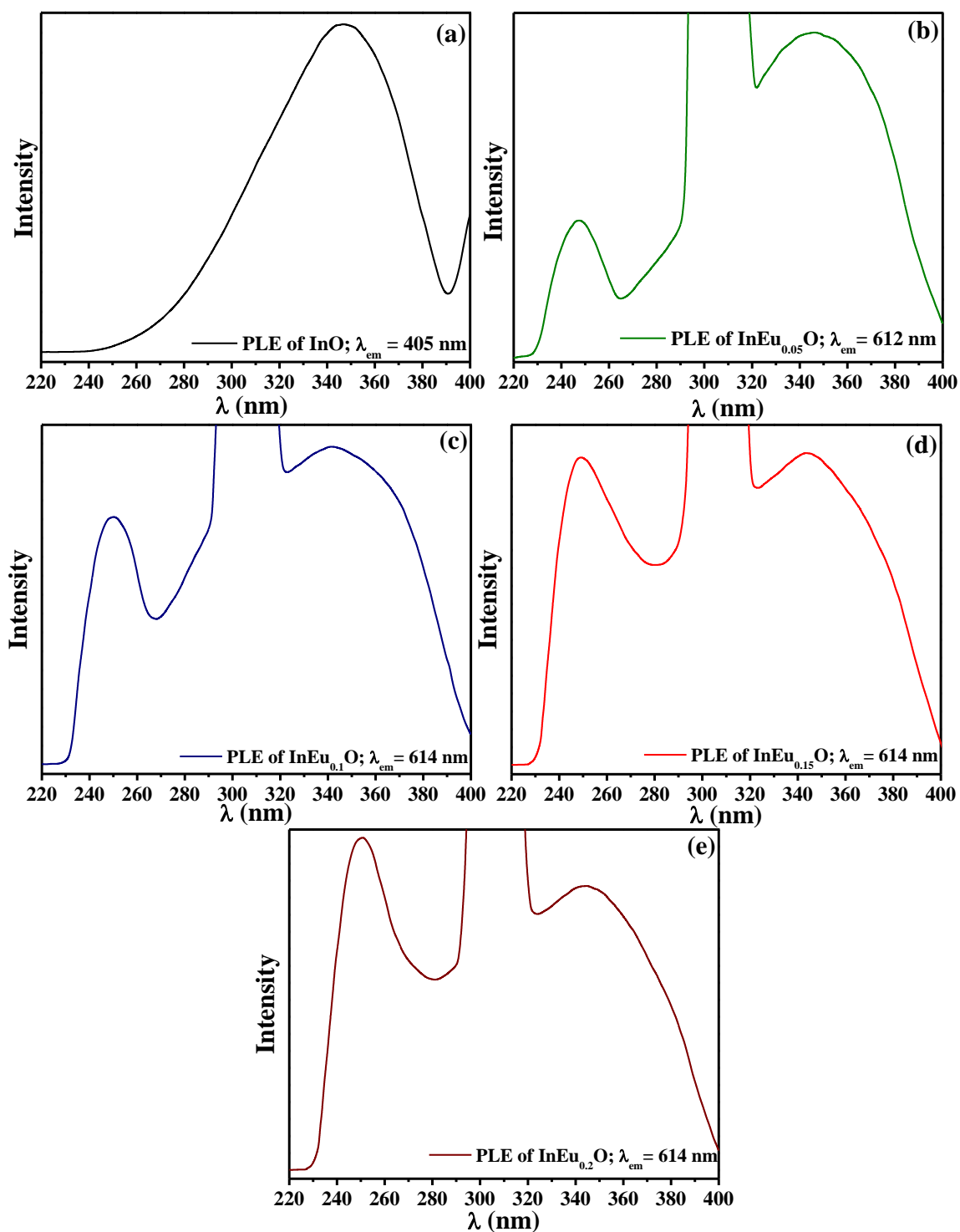


Fig. S7: (a) Excitation spectra of pure In_2O_3 fixing the emission at 405 nm shows a broad excitation band centered at 340 nm which was due to the band gap absorption of In_2O_3 matrix. (b), (c), (d) and (e) also show the excitation spectra of Eu^{3+} doped In_2O_3 NCs at different doping concentrations (5%, 10%, 15% and 20% respectively) fixing the emission wavelength at 614 nm. All the excitation spectra are normalized with respect to same absorbance.

For the doped sample an extra excitation band was present at nearly 245 nm with the host band gap absorption band. The sharp band at 245 nm is associated with the charge transfer from the 2p orbital of O^{2-} to the 4f orbital of Eu^{3+} (Eu-O charge transfer band). The relative intensity of two excitation bands (Eu-O CT band and host band gap excitation) was varied with different doping concentrations. The higher intensity of 340 nm peak clearly indicates that an efficient nonradiative energy transfer (ET) process is occurring from the In_2O_3 host to Eu^{3+} and the excitation efficiency at 340 nm is higher than that at 245 nm for Eu^{3+} emission at 614 nm. In_2O_3 plays a good sensitizer for Eu^{3+} luminescence at doping concentration up to 15%. For $InEu_{0.2}O$ NCs, the intensity of Eu-O CT band is higher than that of host band gap excitation for emission at 614 nm. Direct excitation of Eu^{3+} ions is more susceptible than the ET from host, i.e; larger amount of Eu^{3+} are present at surface of NCs forming a shell of Eu_2O_3 on 20% Eu^{3+} doped InO NCs. That is why there was a decrease in red luminescence in emission profile of $InEu_{0.2}O$ NCs upon excitation at 340 nm.

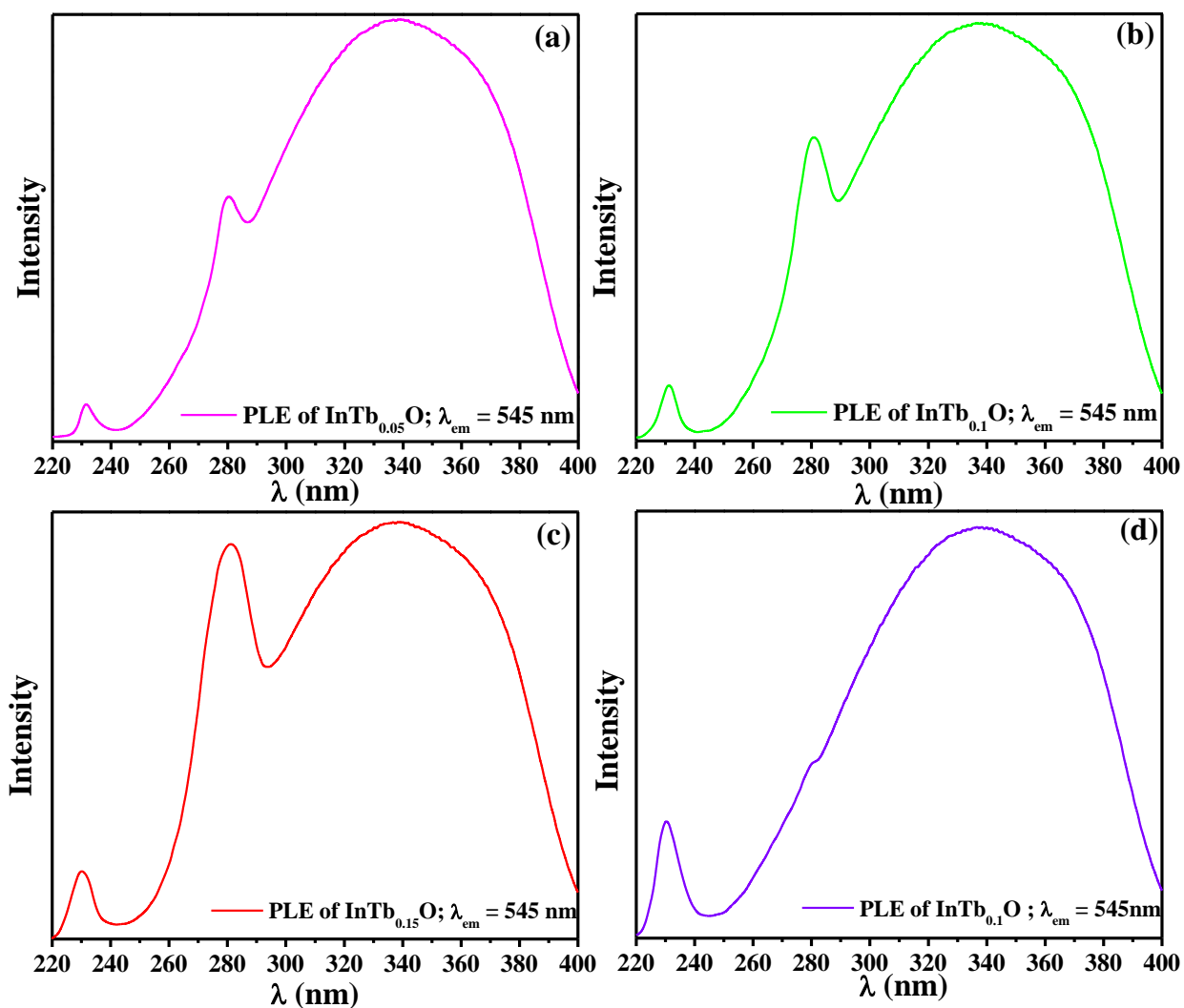


Fig. S8 (a), (b) and (c) are the PLE spectra of InTb_{0.05}O, InTb_{0.1}O and InTb_{0.15}O NCs respectively. Figure (d) shows the excitation spectrum of small InTb_{0.1}O NC. All the excitation spectra are normalized with respect to same absorbance.

Fig. S8 shows the excitation spectra of Tb doped In₂O₃ NC at different Tb doping concentration. The excitation band related to In₂O₃ matrix became much broader on doping due to the formation of larger number of inter-band electronic states (trap states resulting from defects). Fig. S8 (a), (b) and (c) are the PLE spectra of InTb_{0.05}O, InTb_{0.1}O and InTb_{0.15}O NCs respectively. Along with band gap excitation peak, two sharp band at 230nm and 280 nm were present for all the Tb doped NCs.

Both the bands were originated from 4f-5d transitions of Tb^{3+} . Meng et. al² experimentally concluded that the band at 230 nm is due to $4f^8 \rightarrow 4f^7 5d^1$ transition of Tb^{3+} on the surfaces of the NCs and the band at 280 nm is due to similar transition of Tb^{3+} occurred at the interior of NCs. When the doping concentration was increased, the intensity of band at 280 nm enhances significantly with a little enhancement of intensity for the band at 230 nm. Energetically as well as statistically higher amount of surface doping is feasible in the smaller NCs. Doping of Tb^{3+} increased the size distribution of doped NCs (ranges from 10 to 30 nm). Presence of higher concentration of Cl^- in solution increases the population of large NCs than the small one (due to more LLP and oriented attachment). So at higher doping %, as the number of large NC increased, internal doping of Tb^{3+} is more feasible than the surface doping. This is why band at 280 nm enhances on doping with a little change in 230 nm. To verify our speculation we performed size selective precipitation of $InTb_{0.1}O$ NCs to separate out the smaller NCs. Fig. S8 (d) shows the excitation spectrum of small $InTb_{0.1}O$ NCs. The spectrum shows the presence of only 230 nm bands with enhanced intensity and a hump like band at 280 nm. For all the Tb doped NCs, In_2O_3 plays a very good sensitizer matrix as excitation efficiency of 340 nm band is higher than that of other band.

Emission of $\text{InTb}_{0.1}\text{Eu}_{0.1}\text{O}$:

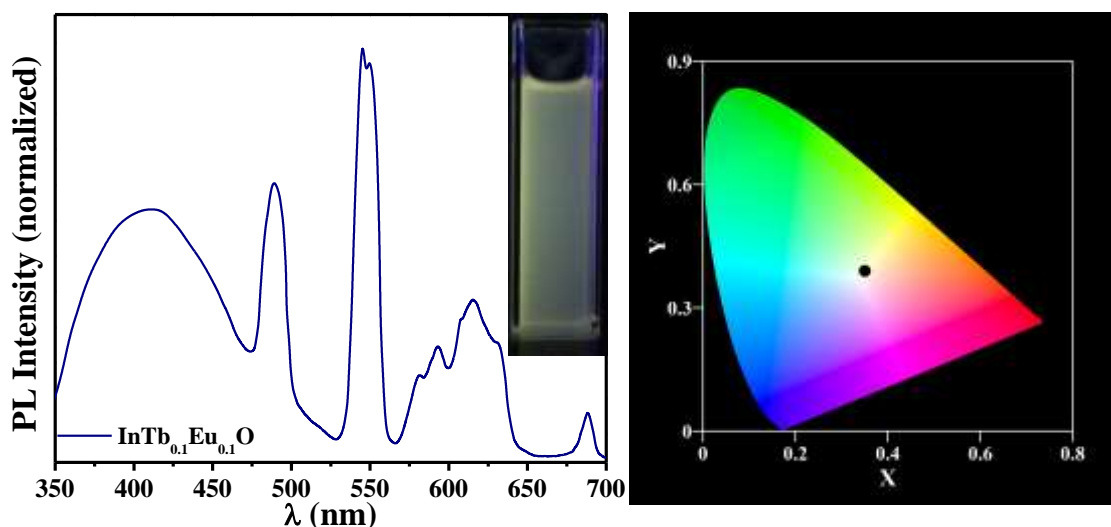


Fig. S9 shows the emission spectrum of $\text{InTb}_{0.1}\text{Eu}_{0.1}\text{O}$ NCs under 340 nm excitation. Inset shows the photograph of the sample dispersed in n-hexane. The calculated chromaticity co-ordinates are 0.35 (X) and 0.39 (Y).

Experimental description and verification of ligand exchange via FTIR:

The ligand exchange process (mass action driven ligand exchange) was used to replace the long chain TOPO by short chain formic acid under ambient condition. Purified colloidal nanocrystals were taken in minimum volume of hexane (10mg/ml). 10 ml 1(M) solution of formic acid in acetonitrile was added to it. The two layer mixture was shaken mildly for 20 minutes. The formic acid capped nanocrystals were precipitated at the bottom of test tube. The precipitate was washed through centrifugation with (1:1) mixture of acetonitrile and ethanol to remove excess formic acid and TOPO. The washing process was repeated for two times. The formic acid capped NCs were well dispersed in ethanol solution.

Fig. S10 shows the FTIR spectra of TOPO and HCOOH capped NCs. The FTIR spectra clearly indicate the presence and proper surface binding of TOPO molecules on NCs. For free TOPO molecules, a sharp characteristic P=O vibration mode appears at 1147 cm^{-1} .³ The P=O

vibration mode for TOPO in capped NCs appeared at 1041 cm^{-1} and it was highly broadened which clearly shows the strong binding of TOPO with In^{3+} ions on NC surface. The stretching vibration of C-H bond of $-(\text{CH}_2)_7\text{-CH}_3$ is appeared between 2800 cm^{-1} and 3000 cm^{-1} . The broad transmittance between 720 cm^{-1} and 2200 cm^{-1} is appeared due to P=O stretching vibrations of TOPO. The formic acid capped NC show FTIR peaks at 1366 cm^{-1} and 1569 cm^{-1} which is due to the $\nu_s(\text{COO})$ and $\nu_{as}(\text{COO})$ vibrations of absorbed formate.⁴

Another significant IR peak is found at 2762 cm^{-1} is owing to $\nu(\text{CH})$ or overlap of $\nu_s(\text{COO})$ and $\delta(\text{CH})$ modes.⁵⁻⁷ $\Delta\nu_{as-s}$ for formic acid capped NC is found to be 203 cm^{-1} which indicate a chelating or/and bi-dentate bridging geometry of carboxylate ions on NC surface.⁸ Significant decrease in intensity of $\nu_{(\text{C-H})}$ is also observed in formic capped NC clearly confirmed maximum removal of TOPO from NC surface. The digital picture in Fig. S10 displays the phase transformation of doped colloids from hexane layer (top layer) to acetonitrile (down layer) during the ligand exchange process under illumination of 365 nm UV excitation source.

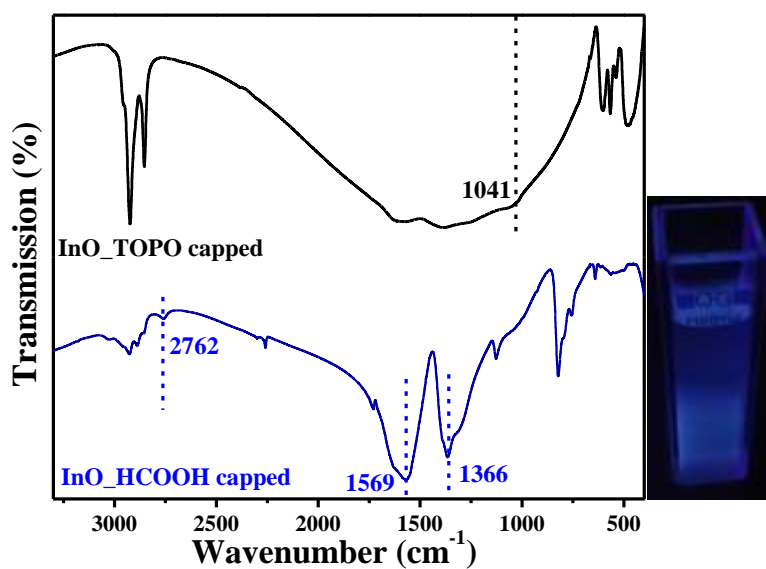


Fig. S10

References:

1. B. Li, Y. Xie, M. Jing, G. Rong, Y. Tang, and G. Zhang, *Langmuir*, 2006, **22**, 9380.
2. Q. Meng, B. Chen, W. Xu, Y. Yang and X. Zhao, *J. Appl. Phys.* 2007, **102**, 093505.
3. B. V. Holt, S. Kudera, A. Weiss, T. E. Schrader, L. Manna, W. J. Parake and M. Braun, *J. Mater. Chem.*, 2008, **18**, 2728.
4. F. P. Rotzinger, J. M. Kesselman-Truttman, S. J. Hug, V. Shklover and M. Gratzel, *J. Phys. Chem. B* 2004, **108**, 5004.
5. G. J. Millar, C. H. Rochester and K. C. Waugh, *J. Catal.* 1995, **155**, 52.
6. M. Calatayud, S. E. Collins, M. A. Baltana's and A. L. Bonivardi, *Phys. Chem. Chem. Phys.* 2009, **9**, 1397.
7. M.-T. Chen, Y.-S. Lin, Y.-F. Lin, H.-P. Lin and J.-L. Lin, *J. Catal.* 2004, **228**, 259.
8. S. Ghosh, K. Das, K. Chakrabarti and S. K. De, *Dalton Trans.*, 2013, **42**, 3434.